EARTH SURFACE PROCESSES AND LANDFORMS
Earth Surf. Process. Landforms **40**, 1043–1056 (2015)

Published online 28 January 2015 in Wiley Online Library
(wileyonlinelibrary.com) DOI: 10.1002/esp.3704

Measurements of the initiation of post-wildfire runoff during rainstorms using *in situ* overland flow detectors

John A. Moody[1]* and Richard G. Martin[2]
[1] US Geological Survey, National Research Program, Boulder, CO, USA
[2] Martin Enterprise, Wheat Ridge, CO, USA

Received 12 August 2014; Revised 23 December 2014; Accepted 8 January 2015

*Correspondence to: John A. Moody, US Geological Survey, National Research Program, Boulder, CO, USA. E-mail: jamoody@usgs.gov

ESPL
Earth Surface Processes and Landforms

ABSTRACT: Overland flow detectors (OFDs) were deployed in 2012 on a hillslope burned by the 2010 Fourmile Canyon fire near Boulder, Colorado, USA. These detectors were simple, electrical resistor-type instruments that output a voltage (0–2·5 V) and were designed to measure and record the time of runoff initiation, a signal proportional to water depth, and the runoff hydrograph during natural convective rainstorms.

Initiation of runoff was found to be spatially complex and began at different times in different locations on the hillslope. Runoff started first at upstream detectors 56% of the time, at the mid-stream detectors 6%, and at the downstream detectors 38% of the time. Initiation of post-wildfire runoff depended on the time-to-ponding, travel time between points, and the time to fill surface depression storage. These times ranged from 0·5–54, 0·4–1·1, and 0·2–14 minutes, respectively, indicating the importance of the ponding process in controlling the initiation of runoff at this site. Time-to-ponding was modeled as a function of the rainfall acceleration (i.e. the rate of change of rainfall intensity) and either the cumulative rainfall at the start of runoff or the soil–water deficit.

Measurements made by the OFDs provided physical insight into the spatial and temporal initiation of post-wildfire runoff during unsteady flow in response to time varying natural rainfall. They also provided data that can be telemetered and used to determine critical input parameters for hydrologic rainfall–runoff models. Copyright © 2015 John Wiley & Sons, Ltd.

KEYWORDS: unsteady overland flow; time-to-start of runoff; initial abstraction; wildfire; infiltrability; convective rainstorms; threshold; hydrologic model parameter

Introduction

Knowing the time from the start of rainfall to the peak runoff discharge is central to forecasting floods. This is especially true in burned areas in steep mountainous terrain where land and emergency managers need advance warning and where this time is frequently shortened substantially by the effects of wildfire. Before runoff can begin, rainfall must first satisfy 'initial losses' related to interception, infiltration, surface depression storage, and any travel time from a source area. These initial losses are often referred to as the initial abstraction, I_a (in millimeters), (Natural Resources Conservation Service, 2004; Springer and Hawkins, 2005), and I_a represents a critical threshold for runoff generation. The rainfall minus I_a is the excess rainfall (Figure 1), which has been used extensively in rainfall–runoff models (e.g. Henderson and Wooding, 1964; Woolhiser, 1975; Dunne and Dietrich, 1980; Julien and Moglen, 1990).

Historically, time-of-concentration, T_C (in minutes), (Figure 1) rather than lag time, T_L (in minutes), has been used to predict runoff volumes based on the unit hydrograph (Natural Resources Conservation Service, 2004, 2010). These two times are difficult to measure and uncertain because one must know either the centroid of mass of the excess rainfall or when the excess rainfall ends, and consequently many empirical equations have been proposed to estimate T_C. However, the time-to-start of runoff, T_r (in minutes), (also referred to as the 'response lag', Carey and DeBeer, 2008) is precise, easy to measure, and is a quasi, real-time parameter because one does not need to know the entire hyetograph or hydrograph as is the case for T_C and T_L (Figure 1). The T_r value is the time from the start of rainfall until the start of runoff, and is given by:

$$T_r = t_i + t_p + t_s + t_t, \quad (1)$$

where t_i (in minutes) is the time for the rainfall to satisfy interception storage by vegetation and by surface litter and duff layers, t_p (in minutes) is the time-to-ponding equal to the time for the initial infiltration to saturate the soil at the surface, t_s (in minutes) is the time to fill surface depression storage on the irregular soil surface (Dunne, 1978; Darboux *et al.*, 2002), and t_t (in minutes) is the travel time from a source point of runoff to a downstream point. Much effort has gone into developing theoretical expressions for t_p (Parlange and Smith 1976; Clothier and White, 1981; Diskin and Nazimov, 1996; Kumke and Mullins, 1997; Chu and Mariño, 2005; Assouline *et al.*, 2007;

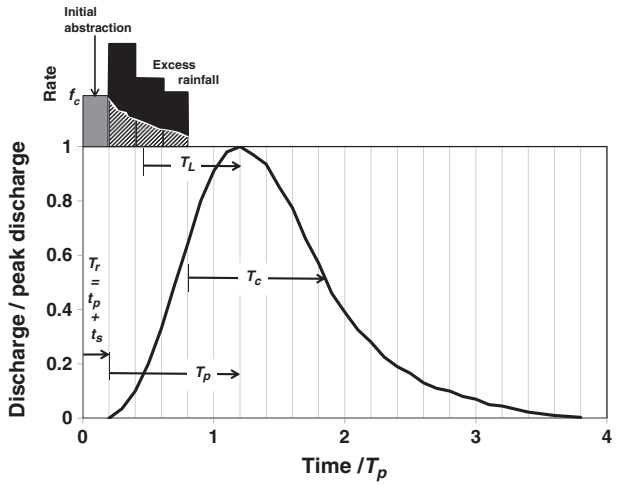

Figure 1. Conceptual diagram of rainfall–runoff parameters. T_p is the time-to-peak measured from the start of the runoff. Time-to-start of runoff, T_r, equals the sum of the interception time, t_i, the ponding time, t_p, the time to 'fill' surface depressions, t_s, and the travel time, t_t. For sources areas of runoff $t_t = 0$, and for burned areas t_i can be assumed ~ zero. The cumulative amount of rainfall, R_p (gray-shaded rectangle in the upper figure) at T_r is equal to the initial abstraction, I_a. At T_r the rainfall intensity equals the infiltrability, f_c. Infiltration rate decreases with time shown by the white line in the upper figure. T_L is the lag time from the centroid of the excess rainfall to the time of the peak discharge. T_C is the time to concentration equal to the travel time from the hydrologically most distant point in a basin to the basin outlet. Modified after National Resources Conservation Service, 2004, 2010.

Xue and Gavin, 2008), but all require a priori knowledge of various soil hydraulic properties (such as minimum and maximum infiltrability, sorptivity, and saturated hydraulic conductivity). Additionally, the rainfall intensity often is constrained to be constant or slowly varying near the ponding time. Time to fill depression storage is a function of the surface roughness and the connectivity of the micro-topography (Antoine *et al.*, 2011). Wildfires can change surface roughness, connectivity, and thus surface depression storage (Moody *et al.*, 2013), and this can have a large impact on runoff (Stone *et al.*, 1995). At runoff sources, $t_t = 0$, and in burned areas t_i is reduced substantially by combustion (but is not zero, i.e. Mitsudera *et al.*, 1984). Thus, for these conditions T_r is essentially the sum of t_p and t_s (Figure 1). By measuring or predicting T_r, one can determine the critical runoff threshold, i.e. I_a, because I_a equals the cumulative rainfall, R_p (in millimeters), at the time, T_r.

Runoff models need to predict the time varying infiltration and the initial abstraction. Infiltration and excess rainfall in most models (e.g. Julien *et al.*, 1995; Hydrologic Engineering Center Hydrologic Modeling System [HEC-HMS], 2000; CASC2D, 2014; KINEROS2, 2014; Water Erosion Prediction Project [WEPP], 2014; WRF-Hydro, 2014) are calculated using either Green and Ampt (1911), Mein-Larson (1973), or Parlange *et al.* (1982) infiltration models. Most infiltration models were developed for agriculture settings and values for critical input variables such as the effective saturated hydraulic conductivity, K_s (in mm h^{-1}) and wetting front suction, S_f (in millimeters), are often unknown for mountainous soils affected by wildfire. The initial abstraction is usually assumed to be 20% of the maximum basin water storage, S (in millimeters), when the curve number method is used (National Resources Conservation Service, 2004). However, publications list a wide range of values for I_a from 5 to 99·6% of S (Ponce and Shetty, 1995; Woodward *et al.*, 2003; National Resources Conservation Service, 2004; Hawkins *et al.*, 2010; Yuan *et al.*, 2014). Appropriate curve numbers for burned areas are still uncertain (Springer and Hawkins, 2005; Foltz *et al.*, 2009) and may, like I_a, also vary with time (Cydzik and Hogue, 2009). Another method is to estimate I_a by calibrating the model using optimization and measured runoff (Cydzik and Hogue, 2009; Alonistioti *et al.*, 2011; Yuan *et al.*, 2014). For low-relief, unburned basins typical values of I_a range from 2.5 to 50 mm (Carey and DeBeer, 2008; Huizinga, 2014) depending upon the environment. For an unburned, forested basin in the southern California mountains, typical calibrated values of I_a ranged from 50·5 to 210 mm (Cydzik and Hogue, 2009).

Under ideal conditions of spatially uniform soil-hydraulic properties, the time-to-start of infiltration-excess overland flow at each point on a hillslope is simultaneous. This begins when the rainfall intensity exceeds a threshold equal to the maximum infiltrability, f_c (in mm h^{-1}), which depends on initial soil–water content, θ_i (in cm^3 cm^{-3}), and soil hydraulic properties (Smith, 2002; Liu *et al.*, 2011). However, soil-hydraulic properties are rarely uniform, and the partial-area conceptual model introduced spatially variable infiltration properties such that runoff could start first down slope near stream channels (where the soil–water content might be higher) and then start later farther upslope (Betson, 1964). Field observations have indicated that under some conditions runoff started upslope, then at mid-slope but 'was not initially continuous' (Bryan *et al.*, 1978, p. 156) or infiltrated before reaching 'a belt extending at the base of the slope area' (e.g. Yair *et al.*, 1980, p. 243) adjacent to the channel. The complexity of runoff in semi-arid landscapes has been described qualitatively as being 'generated patchily' (Kirby, 2011, p. 3), as 'potentially chaotic' (Phillips, 1992, p. 191), or 'scattered across the hillslope' (Srinivasan *et al.*, 2002, p. 649). Later, numerical models addressed some of this spatial complexity in infiltration patterns and in the resulting overland flow (e.g. Woolhiser *et al.*, 1996). Overland flow on hillslopes has been described as a braided or anastomosing flow superimposed on a much slower moving thin film of sheet flow (Emmett, 1970; Dunne and Dietrich, 1980). The deeper, faster braided flow is between surface obstructions and within subtle topographic depressions, which have been referred as 'micro-valleys', 'lateral concentrations' (Emmett, 1970, pp. A13 and A27) or 'microchannels' (Smith and Goodrich, 2005, p. 1715). We referred to these as micro-drainages because they have no distinct banks but widths (between inflection points of profiles orthogonal to the flow) of 5 to 20 cm and depths of 1 to 10 cm. Sheet flow is confined to the interfluvial surfaces between micro-drainages and these surfaces will be referred to as hillslope facets.

In the past, measurements of overland flow have been made during constant rainfall simulations, steady-state equilibrium flow, or overland flow simulations. These have been made in laboratory flumes (e.g. Emmett, 1970; Rauws, 1988; Bunte and Poesen, 1994; Abrahams *et al.*, 2001); in the field using either rainfall simulation (e.g. Emmett, 1970; Dunne and Dietrich, 1980; Abrahams and Parsons, 1991; Gilley *et al.*, 1992; Kinner and Moody, 2010) or overland flow simulation (e.g. Abrahams *et al.*, 1986; Abrahams and Parsons, 1991; Parson *et al.*, 1996; Sheridan *et al.*, 2007; Robichaud *et al.*, 2010; Nyman *et al.*, 2013), and a few have used both types of simulations (e.g. Dunne and Aubry, 1986). Fewer measurements have been made during natural rain storms, which create unsteady flow (e.g. Esteves *et al.*, 2000; Bartley *et al.*, 2006; Bautista *et al.*, 2007; Sen *et al.*, 2010; Orchard, 2013), and no studies to our knowledge have been made on burned hillslopes during unsteady flow.

Few studies have focused specifically on measuring and predicting time-to-start of runoff but none in post-wildfire environments. Thus, the purpose of our research was to understand the spatial and temporal controls on the time-to-start of runoff and hence the initial abstraction for fire-affected soils during

temporally variable rainfall. To achieve this we: (1) developed an overland flow detector (OFD) to measure the time-to-start of runoff and initial runoff velocities, (2) investigated the spatial pattern of the initiation of runoff, and (3) used field observations to test two hypotheses that relate the time-to-start of runoff from fire-affected soils with rainfall characteristics and soil–water properties.

Methods

Field site

The research site was within an area burned by the 2010 Fourmile Canyon fire in the Front Range Mountains near Boulder, Colorado, USA. The site was a north-facing hillslope, which had burned at high intensity (Ebel *et al.*, 2012; Moody and Ebel, 2012a, 2012b, 2013, Figure 1), and contained a small basin (8440 m^2) (Figures 2 and 3) at an elevation of about 2400 m dominated by lodgepole pine (*Pinus contorta*). Two reasons for using this site were: (1) to ensure that a runoff response to unsteady rainfall could be measured, which would probably not be possible in an unburned site; (2) to take advantage of previous research results (Ebel *et al.*, 2012; Moody and Ebel, 2012a, 2012b, 2013).

Figure 2. Upper. The general location of the six overland flow detectors (model 3) are shown as red rectangles (upper site was just over the horizon enclosed by the upper rectangle) on a north-facing hillslope burned by the 2010 Fourmile Canyon fire. The research site is located on the Sugarloaf ridge in the Fourmile Creek basin, which is part of the Front Range Mountains near Boulder, Colorado. The fire started on 6 September 2010 and photograph was taken in October 2010. Lower. View looking down the hillslope showing where the upper group of overland flow detectors were deployed. Black cylinder to the left of the large boulder is flume 1–3. Micro-drainages are highlighted by ponded water. Photograph taken by B. Ebel, 2 August 2011. This figure is available in colour online at wileyonlinelibrary.com/journal/esp

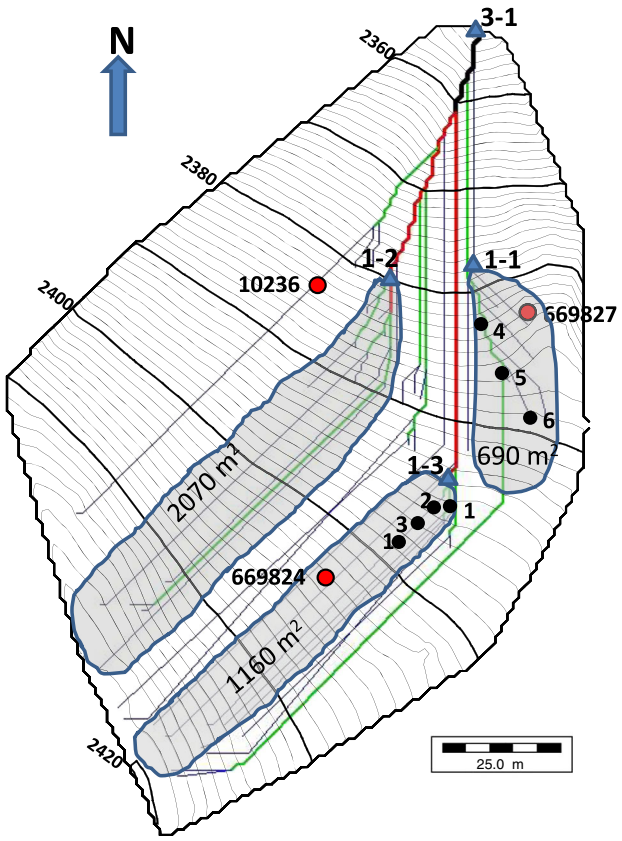

Figure 3. Research basin on the east ridge of Sugarloaf Mountain. Total basin area is 8440 m^2. Drainage network was generated using River Tools (RIVIX, LLC; http://rivix.com) based on elevations measured along transects that approximated the contours and were spaced about 5 m apart. Elevations are relative to the outlet of the research basin at 2354 m above sea level. Recording tipping bucket rain gages are solid red circles and flumes are blue triangles. Flume 3–1 is a 3-inch flume and the other flumes are 1-inch flumes. Flume 3–1 was in place during 2011 and flumes 1–1, 1–2, and 1–3 were added in 2012. Rain gage 669824 was in place in 2011 and gages 669827 and 10236 were added in 2012. Difference infiltrometers were locate at rain gages 669824 and 10236. Overland flow detectors deployed in 2012 are shown as small, solid black circles with their number. Green lines are drainage with a Strahler order of one, red lines are order two, and black line is order three. The shaded areas represent estimates of the contributing area observed in the field and not the total possible drainage area. This figure is available in colour online at wileyonlinelibrary.com/journal/esp

Gravelly sand soils in the site are derived from a bedrock geology that is primarily Boulder granodiorite. They are within the Allens Park member of the Fern Cliff–Allens Park–Rock outcrop complex (Moreland and Moreland, 1975), which are frigid Lamellic and typic Haplustalfa (USDA, 2010; Ebel *et al.*, 2012). In 2011, K_s was estimated using an inverse method and a one-dimensional (1D) infiltration model (Moody and Ebel, 2013). The geometric mean value of K_s for these soils after the wildfire was 1.8 and 0.44 mm h^{-1} for the upper layer (4–9 mm) and lower layer (>9 mm), respectively (Moody and Ebel, 2013).

The area surrounding the research site has a Continental climate (Pepin, 2000) where the precipitation is primarily a mix of cyclonic storms in the spring and fall, convective storms in the summer, and snowstorms in late fall through early spring. Convective storms during the summer are typically high-intensity (>25 mm h^{-1}), short-duration rainfall (10–60 minutes) from storms with monsoon moisture originating from the Gulf of California (Ebel *et al.*, 2012; Douglas

et al., 2004). These storms often consist of a series of cells defined as continuous rainfall with intervals of 'no rain' lasting less than one hour (Moody and Ebel, 2013), and are designated with an A, B, etc. after the date.

Overland flow detection

The OFDs were electrical resistor-type instruments that were relatively inexpensive (*c.* ~$150 in 2011) and simple to construct. They output a voltage (0–2·5 V) and were designed to measure the time of runoff initiation and the runoff hydrograph during natural rainstorms. Resistance detectors have been used to measure the timing or onset (i.e. change from 'no flow' to 'flow') of streamflow (Blasch *et al.*, 2002; Srinivasan *et al.*, 2002; Goulsbra *et al.*, 2009) in ephemeral channels. The current model of the OFD represents a modification of an earlier model designed for and used by Schmidt *et al.* (2011) to measure water depths. These detectors differ from the 'flow–no flow' type and the type that capture a small sample volume (Kirkby *et al.*, 1976; Zimmermann *et al.*, 2014) by measuring a time series signal that is proportional to the runoff depths.

Technical description

OFDs recorded the time-to-start of runoff as a rapid voltage drop. Detectors had three common electrodes (165-mm long and threaded at one end) that also served as support 'legs' and one sensing electrode (127-mm long). All electrodes were 3·2-mm diameter, 303 or 304 stainless steel rods. Common electrodes were mounted in a flat, '3-inch', plastic (PVC) bottom cap at the vertices of an equilateral triangle (Figure 4B, 71·1-mm diameter bolt circle) and electrically connected together. The sensing electrode was mounted in the center of the triangle and connected to a voltage pulse generated by the four-channel data logger (model U12-006, Onset Corp., Bourne, MA). This pulse (2·5 V) was impressed across a half-bridge circuit (upper part was a fixed ~10 kΩ resister) and the measured voltage across the electrodes generated an electrical signal related to the water depth. When the sensing electrode was not in contact with water, the base voltage was 2·5 V, and when it was in contact the voltage drop was proportional to the water depth. Laboratory calibration indicated that the water depth was a linear function of the voltage drop (R^2 values ranged from 0·93 to 0·96 for water depths < 10 mm and from 0·97 to 0·99 for depths < 5 mm). The proportionality constant depends on the specific conductance of the water. We did not measure the specific conductance of the runoff water for each storm so we could not compute absolute water depths, but illustrate the hydrograph as a voltage-drop 'hydrographs', for which relative changes during each storm represent relative changes in water depth.

Field deployment

Six OFDs where deployed in two groups of three detectors in micro-drainages on the burned hillslope. The upper group (OFDs 1, 2, and 3) was located in micro-drainages with slopes ranging from 0·25 to 0·29 (Figure 3A, Table I). These micro-drainages were relatively wide (100–120 cm) and shallow (4–5 cm) at the location of the OFDs, and the bed had a relatively uniform surface texture of fine to coarse sand with only occasionally roots crossing the micro-drainage. Originally, the detectors were placed on two different micro-drainages whose flow lines joined and contributed flow to a '1-inch' Parshall flume (1–3 in Figures 2 (upper) and 3). Later OFD#1 was relocated to the same micro-drainage as OFD#2 and OFD#3 to provide an additional pair of points for measuring velocity. The lower group (OFDs 4, 5, and 6) was located along a single micro-drainage (slopes ranging from 0.26 to 0.51) that contributed flow to a '1-inch' Parshall flume (1–1 in Figure 3). This micro-drainage tended to be narrower (60–160 cm) and deeper (2–12 cm) than the upper micro-drainages. The bed was rougher with outcrops of cobbles and roots creating a 'step-pool' system on the order of 2 to 5 m

Table I. Downhill location of overland flow detectors (OFDs) on the hillslope

OFD#	Distance above flume (m)	Elevation (m)	OFD pair	Separation distance (m)	Slope
1[a]	4·9	2394·54	—	—	—
flume	0·0	2393·22	—	—	0·27
1[a]	18·8	2398·28	—	—	—
3	10·4	2396·18	1-3	8·4	0·25
2	5·2	2394·67	3-2	5·2	0·29
flume	0·0	2393·22	—	—	0·28
6	35·5	2381·43	6-4	21·0	—
5	24·6	2375·86	6-5	10·9	0·51
4	14·5	2373·24	5-4	10·1	0·26
flume	0·0	2366·47	—	—	0·47

Note: OFDs depolyed in the area burned by the 2010 Fourmile Canyon fire were checked, downloaded, and re-launched every day; the sampling interval was one second.

[a]Initially this detector was by itself in a separate micro-drainage 4·9 m uphill from the flume 1–3, but was moved 7·4 m uphill from OFD#3 on 8 July 2012.

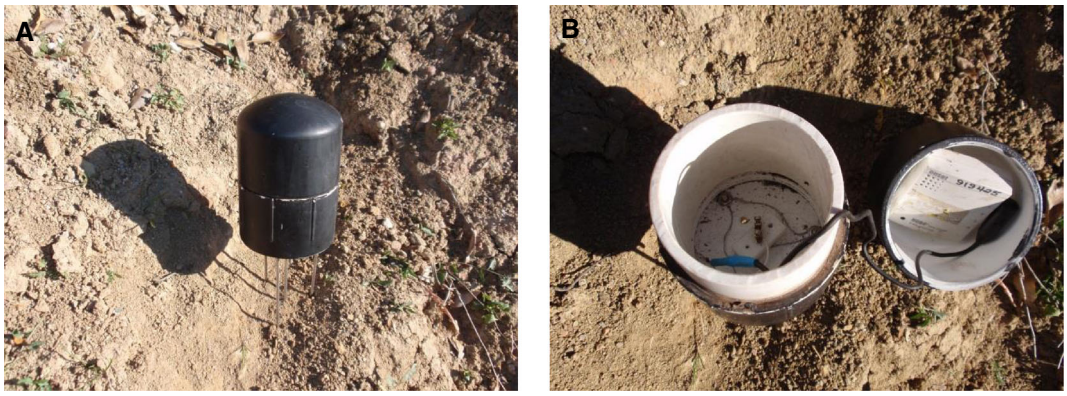

Figure 4. Overland flow detector-model 3. This model is self contained with the data logger (U12-006 Onset corp.) inside a 3-inch PVC housing and therefore avoids having to run wires across the hillslope. It has three (3-mm diameter, stainless steel rods) 'legs' for support, which penetrate the ground and one 3·2-mm diameter stainless steel sensing electrode that is deployed to be about 1 mm above the ground surface. A 76-mm piece of PVC (or ABS) 3 inch diameter pipe was inserted and sealed into the bottom cap to house the data logger (not water proof or water resistant), and a domed, 3-inch PVC cap completed the water proof overland flow detector. This figure is available in colour online at wileyonlinelibrary.com/journal/esp

between steps. OFD#5 was located at the confluence with another micro-drainage. These micro-drainages contributed to a first-order hillslope channel gaged by a '3-inch' modified Parshall flume (3–1 in Figure 3).

Sampling interval was set to one second to adequately resolve the initiation of flow and flow velocities. The clock for each data logger was reset each day to the same identical time (within one second using a global positioning system [GPS] satellite signal). Typical hillslope velocities over bare soil could be on the order of 5 to 50 cm s^{-1} and travel times between pairs of OFDs could range from 10 to 200 seconds (see Table I for distances between detectors) so that by using this sampling interval the uncertainty of the velocity was ~0·5–10%. The sampling interval for the flumes was 10 seconds such that the uncertainty of the velocity between the last detector and the flume was ~5–100% and these velocities were not calculated. For this reason OFD#1 (initially alone in a single micro-drainage) only provided information on the initiation of runoff and no estimates of overland flow velocities. At a one second sampling interval the memory of the data logger (U12-006, Onset Corp.) was filled in about 12 hours. Therefore, the OFDs were downloaded and re-launched each day in the late morning so that they could record the afternoon and evening runoff from summer convective storms. Daily downloading and re-launching served to ensure the quality of the data by inspecting the detectors, cleaning off trash that may have collected during runoff, and re-positioning the sensing electrode (to be within 1 mm of the bed of the micro-drainage) to compensate for any soil erosion under the electrode or soil deposition around the electrode.

Ancillary data

Soil–water content

Surface soil–water content was measured daily by collecting soil cores. Four soil cores (4·7-cm diameter, 1·5-cm long) were collected each morning from a small area (0·1 m × 0·1 m) within a larger area (2 m × 2 m) at two locations near rain gages 669824 and 10236 (Figure 3), placed in soil cans, sealed, and the volumetric soil–water content, θ (in cm^3 cm^{-3}) was determined thermogravimetrically in the laboratory (Topp and Ferré, 2002). Subsurface arrays measured temperature and θ (model 5TE, Decagon Devices, Pullman, WA) every minute at four depths (0·05, 0·10, 0·15, and 0·20 m), and had been deployed since 2010. When these sensors were deployed, soil samples were collected to determine saturated soil–water content, θ_s (in cm^3 cm^{-3}) which was 0·49 cm^3 cm^{-3}, and the van Genuchten soil hydraulic parameters (van Genuchten *et al.*, 1991; Ebel *et al.*, 2012; Moody and Ebel, 2013).

These soil cores provide an estimate of the initial soil–water content, θ_i (in cm^3 cm^{-3}), for the first rain cell A (Table II). For succeeding storm cells (B and C) during a convective storm, θ_i was estimated by using the Hydrus-1D numerical infiltration model (Šimùnek *et al.*, 2008; Moody and Ebel, 2013). This model requires the initial subsurface soil–water profile at the start of rainfall, θ_s, van Genuchten soil-hydraulic parameters, and the observed hydrograph near the sub-surface sensor array (see Moody and Ebel, 2013, for details). The observed hydrograph was recorded by the runoff gages associated with the rain gages at 669624 and 10236 (Figure 3; Moody and Ebel, 2012b).

Rainfall characteristics

Three rainfall characteristics (cumulative rainfall, rainfall intensity, and rainfall acceleration) were computed from data collected by three rain gages. These were 15-cm diameter, tipping-bucket gages (see locations in Figure 3) with each tip equal to 0·254 mm, a data logger that recorded the time of each tip (HOBO, Onset Corp.), and installed ~1 m above the ground. They were inspected, downloaded, and re-launched about every 14 days to ensure that there were no obstructions and that the total clock drift (~2–3 seconds day^{-1}) was minimal. One-minute rainfall intensities, $I_1(t)$ (in mm h^{-1}), were computed by first interpolating the irregular time series of 'tip times' to a regular interval of 0.1 minute, and then computing a one-minute backwards difference from the interpolated cumulative rainfall values. The rainfall acceleration, a (in mm h^{-2}), was the slope of the least-squares standard linear regression line ($I_1(t)$ versus t) from the start of rainfall at $t = 0$ when $I_1(0) = 0$ to the time of peak rainfall intensity (Moody and Ebel, 2013).

Time-to-start of runoff

Time-to-start of runoff in the micro-drainages was measured by the OFDs and on hillslope facets it was measured at the two difference infiltrometers. Each difference infiltrometer (669824 and 10236 in Figure 3) consisted of a tipping-bucket rain gage and a runoff plot (radius ~ 0·25 m) with a runoff gage. Because the runoff plots were small, the travel time, t_t, and the time-to-fill the surface depressions, t_s, were negligible compared to the time-to-ponding, t_p (Moody and Ebel, 2012b, 2013). Thus, measurements of t_p provide estimates of T_r on the hillslope for comparison with T_r values in the micro-drainages.

Overland flow velocities

Overland flow velocities were simulated (during periods with no rain) in micro-drainages on the same hillslope where the OFDs were deployed. Water was released from a 20-l jug at a maximum rate of 0·05 l s^{-1} and velocity was computed from the travel time of dye or particles in the water between two points separated by a known distance. These velocity measurements were used for comparison with the OFD flow velocities and with flow velocities measured using the same method in the area burned by the 2005 Harvard Fire near Burbank, California (Table III).

Analysis

Analysis was limited by the number of the convective rainstorms during the summer of 2012. Most storms were during two narrow windows from 5 to 12 July and from 27 to 30 July. The dataset consisted of hydrographs generated by 10 separate storm cells on 5, 6, 7, 8, 12, 27, 29 and 30 July 2012 (Table II).

Observed time-to-start of runoff

Observed time-of-start of runoff, T_r, was the elapsed time from the start of rainfall to the start of runoff. Clock time for the start of runoff was measured by the OFDs to within one second; however, clock time for the start of rainfall is not known when tipping-bucket rain gages are used – only the time of the first tip. These start times were estimated by linearly extrapolating back in time, using data for the first three tips. Median value of the 90 and 95% uncertainty limits for the 20 estimated times for the start of rainfall were ± 1·0 and ± 2·0 minutes, respectively. Cumulative rainfall was digitized at 0·1 minute interval. Cumulative rainfall at the start of runoff was determined by interpolation between the 0·1-minute intervals if necessary, and one-minute rainfall intensities, I_1, were computed using these 0·1-minute values.

Table II. Rain and soil characteristics and runoff characteristics measured by overland flow detectors (OFDs) during eight rain storms

OFD#	Rain					Hillslope		Runoff in micro-drainage						Velocity (cm s^{-1})		
	Start of rain	Duration of rain	Maximum one-minute intensity	Intensity at start of runoff i_r	Rainfall acceleration, a	Initial water content at start of rain, θ_i	Time-to-ponding, t_p	Start of Runoff	Cumulative rainfall at start of runoff, R_p	Observed, T_r	Travel time, t_t	Predicted, t_p	Time of first peak	OFD pair	Leading edge of water	First peak
		(minutes)	(mm h^{-1})	(mm h^{-1})	(mm h^{-2})	(cm^3 cm^{-3})	(minutes)		(mm)	(minutes)	(minutes)	(minutes)				
							5A July 2012									
1	16:01:10	43	101	31·3	290	0·015	3·5	16:02:11	0·41	1·0		2·2	16:16:53	—	—	—
3	16:01:10	43	101	30·8	290	0·015	3·5	16:03:01	0·74	1·9		3·0	16:15:22	—	—	—
2	16:01:10	43	101	30·8	290	0·015	3·5	16:01:48	0·28	0·63		1·9	16:15:32	3-2	—	52
6	16:00:45	41	104	17·8	272	0·018	3·3	16:02:49	0·63	2·1		2·9	16:13:38	—	—	—
5	16:00:45	41	104	26·4	272	0·018	3·3	16:03:36	1·04	2·8	0·8	3·7	16:14:24	6-5	23	24
4	16:00:45	41	104	20·6	272	0·018	3·3	16:06:22	2·36	5·6	2·8	5·6	16:14:54	5-4	6·1	34
							6B July 2012									
1	16:44:43	22	30·4	18·2	160	0·358	4·6	16:51:28	1·28	6·7		5·4	17:05:16	—	—	—
3	16:44:43	22	30·4	9·7	160	0·358	4·6	16:51:50	1·38	7·1		5·6	17:04:51	—	—	—
2	16:44:43	22	30·4	16·6	160	0·358	4·6	16:49:29	0·68	4·8		3·9	17:05:35	3-2	—	12
6	16:44:30	24	27·2	4·8	159	0·361	3·6	16:48:00	0·47	3·5		3·2	17:03:51	—	—	—
5	16:44:30	24	27·2	7·5	159	0·361	3·6	16:47:00	0·37	2·5		2·9	17:05:57	6-5	—	9
4	16:44:30	24	27·2	22·2	159	0·361	3·6	16:45:19	0·14	0·82		1·8	17:07:25	5-4	—	11
							6C July 2012									
1	20:16:50	161	37·0	29·2	63·5	0·402	3·9	20:35:15	2·48	18·4		11·9	20:39:16	—	—	—
3	20:16:50	161	37·0	7·9	63·5	0·402	3·9	20:22:10	0·39	5·3		4·7	20:41:41	—	—	—
2	20:16:50	161	37·0	4·4	63·5	0·402	3·9	20:31:06	1·17	14·3	8·9	8·1	20:42:12	3-2	1·0	17
6	20:13:37	169	43·7	26·9	52·8	0·373	9·7	20:36:26	2·04	22·8		11·8	20:41:20	—	—	—
5	20:13:37	169	43·7	26·0	52·8	0·373	9·7	20:37:09	3·03	23·5	0·7	14·4	20:42:19	6-5	25	18
4	20:13:37	169	43·7	31·1	52·8	0·373	9·7	20:37:03	1·34	23·4		9·6	20:42:19	5-4	—	—
							7B July 2012									
1	14:37:35	134	49·3	12·9	7·00	0·291	43·6	15:21:45	2·06	44·2		32·5	16:40:53	—	—	—
3	14:37:35	134	49·3	6·3	7·00	0·291	43·6	15:24:35	2·44	47·0		35·4	16:41:02	—	—	—
2	14:37:35	134	49·3	6·2	7·00	0·291	43·6	15:19:15	1·55	41·7		28·2	16:43:53	3-2	—	3·1
6	14:39:40	136	69·1	26·7	7·00	0·209	43·6	15:59:07	5·79	79·4		54·6	16:40:04	—	—	—
5	14:39:40	136	69·1	7·3	7·00	0·209	43·6	15:43:15	3·64	63·6		43·3	16:39:47	6-5	—	—
4	14:39:40	136	69·1	18·2	7·00	0·209	43·6	15:57:30	5·17	77·8	14·2	51·6	16:42:05	5-4	1·2	7·3
							8A July 2012									
1	18:21:17	66	49·4	5·9	166	0·305	5·1	18:25:20	0·55	4·1		3·5	18:38:07	—	—	—
3	18:21:17	66	49·4	41·4	166	0·305	5·1	18:27:10	1·5	5·9	1·8	5·7	18:39:47	1-3	7·6	8·4
2	18:21:17	66	49·4	42·1	166	0·305	5·1	18:27:09	1·4	5·9		5·5	18:37:35	3-2	—	—
6	18:20:08	72	46·8	29·5	209	0·206	22·6	18:26:34	1·2	6·4		4·5	18:38:01	—	—	—
5	18:20:08	72	46·8	34·0	209	0·206	22·6	18:26:49	1·4	6·7	0·3	4·9	18:40:55	6-5	73	6·3
4	18:20:08	72	46·8	29·5	209	0·206	22·6	18:26:34	1·2	6·4		4·5	18:42:55	5-4	—	8·4

Table II. (Continued)

OFD#	Rain					Hillslope		Runoff in micro-drainage						Velocity (cm s^{-1})		
	Start of rain	Duration of rain	Maximum one-minute intensity	Intensity at start of runoff i_r	Rainfall acceleration, a	Initial water content at start of rain, θ_i	Time-to-ponding, t_p	Start of Runoff	Cumulative rainfall at start of runoff, R_p	Observed, T_r	Travel time, t_t	Predicted, t_p	Time of first peak	OFD pair	Leading edge of water	First peak
		(minutes)	(mm h^{-1})	(mm h^{-1})	(mm h^{-2})	(cm^3 cm^{-3})	(minutes)		(mm)	(minutes)	(minutes)	(minutes)				
							12A July 2012									
1	16:00:43	11	98·5	19·9	791	0·132	3·1	16:02:22	0·61	1·7		1·7	16:04:58	—	—	—
3	16:00:43	11	98·5	21·8	791	0·132	3·1	16:02:31	0·71	1·8	0·1	1·8	16:06:29	1-3	93	9·2
2	16:00:43	11	98·5	22·1	791	0·132	3·1	16:02:00	0·50	1·3		1·5	16:06:56	3-2	—	19
6	15:58:00	12	82·5	16·8	381	0·119	7·2	16:02:53	0·76	4·9		2·7	16:07:42	—	—	—
5	15:58:00	12	82·5	22·4	381	0·119	7·2	16:03:15	0·93	5·3	0·4	3·0	16:11:13	6-5	50	5·2
4	15:58:00	12	82·5	12·8	381	0·119	7·2	16:03:04	0·82	5·1		2·8	16:12:05	5-4	—	19
							12B July 2012									
1	16:40:17	6·2	70·4	37·0	841	0·459	0·8	16:37:15	0·0			0·0	16:46:17	—	—	—
3	16:40:17	6·2	70·4	37·0	841	0·459	0·8	16:39:41	0·0		2·4	0·0	16:45:37	1-3	5·8	—
2	16:40:17	6·2	70·4	37·0	841	0·459	0·8	16:39:04	0·0			0·0	16:46:18	3-2	—	13
6	16:38:18	8·2	83·7	52·3	502	0·427	1·5	16:40:07	0·41	1·8		1·7	16:45:32	—	—	—
5	16:38:18	8·2	83·7	8·6	502	0·427	1·5	16:40:45	0·50	2·4	0·6	1·9	16:47:28	6-5	29	9·4
4	16:38:18	8·2	83·7	9·9	502	0·427	1·5	16:44:15	2·7	5·9	3·5	4·4	16:50:06	5-4	4·8	6·4
							27A July 2012									
1	11:46:15	22·0	39·4	7·0	62	0·032	17·5	11:56:45	0·76	10·5		6·6	12:06:52	—	—	—
3	11:46:15	22·0	39·4	7·0	62	0·032	17·5	12:06:20	3·65	20·1	9·6	14·6	12:06:43	1-3	1·5	—
2	11:46:15	22·0	39·4	39·4	62	0·032	17·5	11:54:02	0·52	7·8		5·5	12:09:01	3-2	—	3·8
6	11:48:41	55·0	35·3	8·4	72	0·037	17·1	12:02:41	1·90	14·0		9·8	12:05:35	—	—	—
5	11:48:41	55·0	35·3	11·0	72	0·037	17·1	12:04:46	2·62	16·1	2·1	11·5	12:07:07	6-5	8·7	12
4	11:48:41	55·0	35·3	6·7	72	0·037	17·1	12:01:17	1·41	12·6		8·4	12:08:54	5-4	—	9·4
							29A July 2012									
1	14:34:23	25·0	17·3	17·3	180	0·071		14:40:16	1·19	5·9		4·9	14:45:03	—	—	—
3	14:34:23	25·0	17·3	11·6	180	0·071	no runoff at difference infiltrometers	14:41:17	1·38	6·9	1·0	5·3	14:44:10	1-3	14	—
2	14:34:23	25·0	17·3	17·1	180	0·071		14:40:12	1·16	5·8		4·8	14:44:40	3-2	—	17
6	14:35:51	23·0	27·1	8·4	617	0·101		14:37:46	0·58	1·9		1·8	14:43:39	—	—	—
5	14:35:51	23·0	27·1	19·8	617	0·101		14:44:25	2·93	8·6	6·7	4·1	14:45:37	6-5	2·7	9·2
4	14:35:51	23·0	27·1	20·0	617	0·101		14:44:01	2·80	8·2		4·0	14:46:52	5-4	—	13
							30A July 2012									
1	15:18:03	15·5	34·4	9·7	1970	0·147	2·5	15:18:20	0·16	0·28		0·5	15:21:40	—	—	—
3	15:18:03	15·5	34·4	9·7	1970	0·147	2·5	15:18:20	0·16	0·28		0·5	15:21:40	1-3	—	—
2	15:18:03	15·5	34·4	25·6	1970	0·147	2·5	15:20:01	1·00	2·0	1·7	1·4	15:22:19	3-2	5·2	13
6	15:18:12	6·1	76·8	22·5	1680	0·182	1·6	15:18:44	0·38	0·53		0·9	15:23:58	—	—	—
5	15:18:12	6·1	76·8	69·8	1680	0·182	1·6	15:20:46	2·30	2·6	2·0	2·2	15:22:38	6-5	8·9	—
4	15:18:12	6·1	76·8	14·7	1680	0·182	1·6	15:18:33	0·24	0·35		0·7	15:24:53	5-4	—	7·5

Note: saturated for 12B July 2012 indicates that the soil was saturated from rain cell A and enough soil moisture was still present to indicate runoff had started before the rain cell B started; soil–water content at saturation was 0·49 cm^3 cm^{-3}, Moody and Ebel, 2013.

Table III. Simulated overland depth and flow velocities

Source	Conditions	Slope	Depth (mm)	Velocities (cm s^{-1})
Abrahams *et al.*, 1986	Desert soils	0·092–0·687	1·1–7·7	6·6–37
Bunte and Poesen, 1994	Bare soils in flume	0·014	1·3–11	5–18
Emmett, 1970	Semi-arid soils	0·029–0·33	0·2–46	0·18–12
Nyman *et al.*, 2013	Burned soils	0·36–0·40	6–14	62–114
Robichaud *et al.*, 2010	Low burn severity	0·24–0·64	6·3 ± 2·2	7·3 ± 5·8
Robichaud *et al.*, 2010	High burn severity	0·23–0·75	6·5 ± 2·0	31 ± 12
This paper, 2005 Harvard fire	High burn severity, hillslope facets	0·38–0·79	—	8–21
This paper, 2010 Fourmile fire	High burn severity, hillslope micro-drainages	0·18–0·65	—	7–14

Predicted time-to-start of runoff

The T_r value depends partly on time-to-ponding, t_p. Time-to-ponding at the point scale (~1 m^2) on burned hillslopes facets depends on rainfall characteristics more than on fire-affected soil hydraulic properties (Moody and Ebel, 2013). For convective rainfall, an empirical relation was found to predict t_p on burned hillslopes (Moody and Ebel, 2013):

$$t_p = \left(\frac{R_p}{a}\right)^{1/2} \tag{2}$$

Substituting Equation (2) into Equation (1) provides one relation between T_r and rainfall characteristics with the initial assumptions that t_i and t_s are zero. Thus R_p is a posteriori variable known only after runoff begins. If it is assumed to depend on the soil-saturation deficit, $(\theta_s - \theta_i)$ (in cm^3 cm^{-3}), then site-specific relations can be determined to predict the cumulative rainfall, R_p based on a priori variables. Infiltration and runoff are usually non-linear functions of $\theta_s - \theta_i$ (often exponential e.g. Horton, 1939; Smith, 2002), thus data collected from the two difference infiltrometers in 2011 (Moody and Ebel, 2012b, 2013) were used to determine the following empirical soil-saturation deficit equations to predict R_p:

$$2011\ at\ 669824 : R_p = 0{\cdot}93e^{2{\cdot}88(\theta_s-\theta_i)}, R^2 = 0{\cdot}76 \tag{3a}$$

$$2011\ at\ 10236 : R_p = 0{\cdot}59e^{2{\cdot}96(\theta_s-\theta_i)}, R^2 = 0{\cdot}72 \tag{3b}$$

Equation (3a) would apply to OFDs 1, 2, and 3 and equation (3b) to OFDs 4, 5, and 6. Substituting the appropriate soil-saturation deficit equation into Equation (1) provides a second relation between T_r and rainfall characteristics and soil properties.

Flow velocities

Flow velocities in the micro-drainages were calculated from the separation distance between detectors (Table I) and the time difference in arrival of one of two distinct features of the hydrograph. One feature was the relatively rapid initial rise and the second was the first peak (Peak, Table II) in the hydrograph. Several OFD hydrographs had multiple peaks, but peaks after the first peak were not used to determine the velocity because of the possibility of deposition of debris on or erosion beneath the sensing electrode after the first peak. Velocities were only computed between consecutive downhill pairs of detectors (i.e. 1–3, 3–2, 6–5, and 5–4).

Results

Rain and soil–water content

The summer monsoon season was brief in 2012 lasting only from 5 July through 30 July 2012 with essentially no rainfall greater than 5 mm day^{-1} in August. Eight days in July had at least 5 mm of rainfall and average rainfall intensities > 5 mm h^{-1}. These eight days (5, 6, 7, 8, 12, 27, 29, and 30 July) had 10 storm cells with median duration of 25 minutes; a median, maximum one-minute rainfall intensity of 48 mm h^{-1}; and a median rainfall acceleration of 195 mm h^{-2} (Table II). Each storm cell had multiple one-minute intensity peaks (Figure 5) with 7B July having five distinct peaks, but the rainfall was spatially uniform over the research area (Figure 3). Near surface (~1–2 cm) soil–water content, θ_i at the beginning of the monsoon rain season on 5 July 2012 was quite dry (0·015–0·018 cm^3 cm^{-3}, Table II), increased during the first week of rain to a maximum of (0·459 cm^3 cm^{-3}) before rain cell 12B July, and then decreased during the dry period from 13 July to 27 July 2012 down to 0·032–0·037 cm^3 cm^{-3}.

Hydrographs

All OFDs recorded a hydrograph for each storm cell, and the shape of the hydrograph resembled the hyetograph. The rising limb of the hydrographs was relatively gradual and not abrupt as would be expected for the sudden arrival of a flood wave, and there was no obvious dispersion of the peak at the hydrograph downhill. There were exceptions like the sudden abrupt peak for OFD#3 during the 12A July 2012 rain cell (Figure 5A). The falling limb sometimes did not return to zero water depth because small debris caught on the electrode or soil moisture at the surface continued for a while to provide an electrical pathway, which produced a voltage drop. This was one of the reasons for inspecting the OFD detectors daily in order to remove the debris and re-deploy the detectors.

Time-to-start of runoff

The spatial distribution of runoff was complex. Runoff did not start simultaneously on the hillslope and in the micro-drainages. Linear regression between the observed T_r on hillslope facets (T_r = t_p, Table II) and the observed T_r in the micro-drainages (Table II) indicated the T_r on the hillslope was about 20% shorter (R^2 = 0.76) than in the micro-drainages. Observed T_r in the micro-drainages ranged over two orders of magnitude from 0·3 to 79·4 minutes (Table II). In general, T_r in the micro-drainages were inversely correlated (power law, R^2 = 0.54) with rainfall acceleration, a, reflecting the

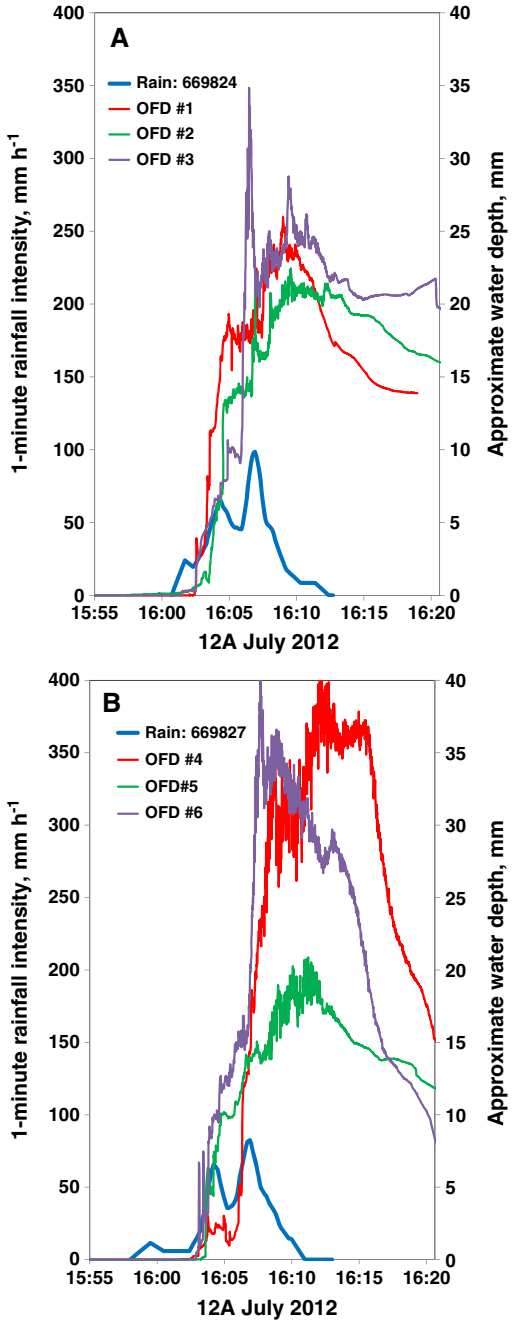

Figure 5. (A) Hyetograph (one-minute rainfall intensities) and hydrographs (one-second voltage drop expressed as approximate 'water depth') for overland flow detectors #1, #2, and #3 during the storm cell 12A July 2012. (B) Hyetograph (one-minute rainfall intensities) and hydrographs (one-second voltage drop expressed as approximate 'water depth') for overland flow detectors #4, #5, and #6 during the storm cell 12A July 2012. This figure is available in colour online at wileyonlinelibrary.com/journal/esp

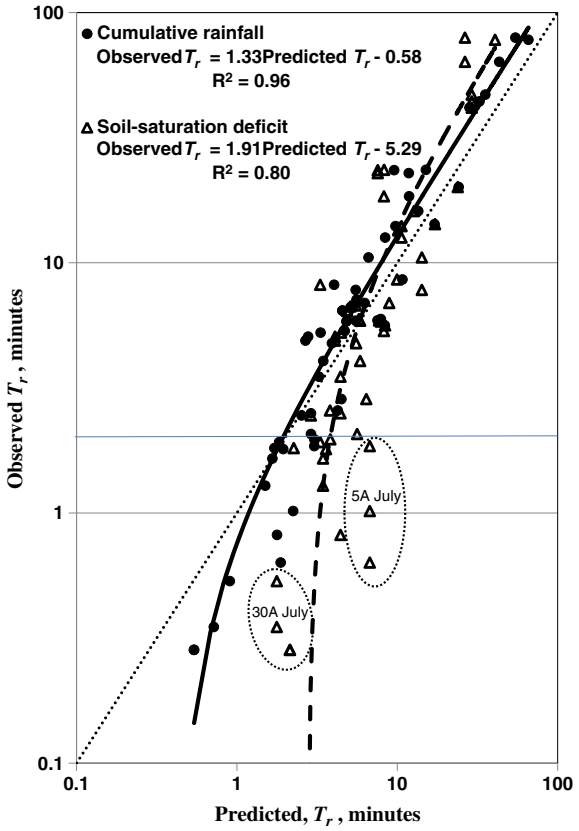

Figure 6. Comparison of predicted and observed time-to-start of runoff, T_r. The dotted line is the line of prefect agreement. Predicted values are based on the cumulative rain at start of runoff (solid line) and on an empirical soil–saturation deficit approximation of the cumulative rainfall (dashed line) based on 2011 data (Equation (3a)). The encircled data represents two extremes when the initial soil–water content, θ_i, was the driest (0·015–0·018 cm^3 cm^{-3}, 5A July 2012) and when the rainfall acceleration, a, was the largest (1680–1970 mm h^{-2}, 30A July 2012).

dependence indicated by Equation (2), but they were not correlated with either θ_i or maximum I_1.

The cumulative-rainfall relation (Equations (1) and (2)) explained 96% of the variance in observed values of T_r. On average, this relation under predicted T_r, but over predicted T_r for values < two minutes (Figure 6):

$$\text{Observed } T_r = 1{\cdot}33 \text{ Predicted } T_r - 0{\cdot}58;\ R^2 = 0{\cdot}96 \quad (4)$$

The soil–saturation deficit relation (Equations (1)–(3)) explained 80% of the variance in T_r:

$$\text{Observed } T_r = 1{\cdot}91 \text{ Predicted } T_r - 5{\cdot}29;\ R^2 = 0{\cdot}80 \quad (5)$$

and on average it also under predicted T_r. The 95% confidence limits for the slope and intercepts for these equations were ± 0·06 and ± 0·22 and ± 1·02 and ± 2·67 minutes, respectively, so that the intercept for the cumulative-rainfall relation (Equation (4)) is essentially zero, whereas the intercept for the soil–water deficit relation (Equation (5)) is not. This bias in the soil–water deficit relation is reflected in the predicted values for $T_r < 2$ minutes, which were over predicted by a factor of 4 to 10 (Figure 6). The largest over predictions correspond to two different extreme conditions (data points are circled in Figure 6) when θ_i was the driest (5A July 2012, Table II) and when a was the largest (30A July 2012, Table II). The 95% confidence limits for the start of the rainfall are ± 2 minutes, and one could justify using only the data for $T_r > 2$ minutes to determine the empirical relations for Equations (4) and (5). This was done and Equations (4) and (5) were essentially unchanged with nearly identical slopes, intercepts, and R^2 values.

Initial abstraction, I_a, and maximum infiltrability, f_c

When travel time is zero, I_a equals measured values of R_p at T_r. The median value of I_a was 0·7 mm for the upper group of OFDs (1, 2, and 3), 1·0 mm for the lower group of OFDs (4, 5, and 6), and the range for the combined groups was from 0·1 to 5·8 mm. Differences in I_a between the upper and lower groups of OFDs for each storm cell were not significantly (two-tail, $p = 0{\cdot}33$). So the mean value of I_a was 1·2 mm (coefficient of variation of 0·94) and is an estimate of the threshold

for runoff initiation at this burned site. These values are usually much lower than typical threshold values published for unburned low-relief areas (2·5 to 50 mm; Carey and DeBeer, 2008; Huizinga, 2014) and for mountainous areas (98·6 mm; Cydzik and Hogue, 2009). Few measurements of I_a exist for burned areas, but for comparison, a 'conservative' lower limit of 1·0 mm was assumed by Elliott *et al*. (2005) to model runoff using the curve number method for the 2002 Hayman fire (also in the Front Range Mountains of Colorado). This was based on a minimum rainfall value observed to generate runoff after wildfires. In contrast, a post-wildfire model calibration value of 19·6 mm was reported by Cydzik and Hogue (2009) for the first year after the 2003 Old fire in the southern California mountains.

The maximum infiltrability can also be determine by knowing T_r when $t_t = 0$, because the rainfall intensity $I_1(t)$ at T_r equals f_c. Median values of f_c were 17·1 and 17·3 mm h^{-1} for the upper and lower group of OFDs, respectively. These, like I_a were not significantly different (two-tail, $p = 0{\cdot}88$) between the upper and lower sites, so the mean value of f_c was 18·9 mm h^{-1} with a coefficient of variation of 0·60. This infiltrability threshold is often expressed as 'rainfall-intensity threshold' and published values for burned areas range from 8·5 to 20 mm h^{-1} (Moody and Martin, 2009).

Flow velocities

Overland flow velocities measured during simulations on hillslope facets and in micro-drainages on the hillslope were comparable. Those on the hillslope facets ranged from 8 to 21 cm s^{-1} and those in the micro-drainages ranged for 7 to 14 cm s^{-1} (Table III). Velocities in micro-drainages were not detected by the OFDs for all storm cells. For 50% of the storm cells the leading edge of the water had velocities that ranged from 1 to 93 cm s^{-1} (Table II) with median values of 5·8 and 8·9 cm s^{-1} for the upper and lower group of detectors. For 78% of the storm cells the hydrograph peak had velocities ranging from 3 to 52 cm s^{-1} (Table II) with median values of 12·8 and 9·4 cm s^{-1} for the upper and lower group, respectively.

Discussion

Initiation of runoff

Based on these few OFD, the initiation of runoff appears to be complex, starting at different times at different locations during different storm cells. Runoff from storm cells started first in micro-drainages (69%) before it started on hillslope facets (31%). Runoff was initiated first at an upstream detector 56%, at the mid-stream detector 6%, and at the downstream detector 38% of the time. As an example of this complex response, flow began first (T_r = 2·1 minutes) during the 5A July 2012 storm cell at OFD#6, then on the lower hillslope facet (T_r = 2·8 minutes), and finally (T_r = 5·6 minutes) at the most downstream OFD#4, which included 3·5 minutes of travel time from OFD#6. A similar pattern of complex response was observed by Kinner and Moody (2010) during rainfall simulations on 1-m^2 plots on hillslopes burned by the 2003 Overland fire in Colorado. They noted ponding first in topographic lows at different locations along the micro-drainage network, which often expanded in the uphill and downhill directions and eventually became connected to form a single body of water flowing downstream.

Whether or not runoff started first on hillslope facets or in micro-drainages did not depend on θ_i ($R^2 < 0{\cdot}1$). However, θ_i was measured at only two sites (669824 and 10236, Figure 3) on the hillslope and not at OFDs sites in the micro-drainages. Thus, one cannot rule out θ_i at the OFDs sites from affecting T_r. This suggests that even at the relatively small scale of this hillslope (~100 m × 200 m), θ_i cannot be characterized by two values. Differences in θ between hillslope and micro-drainage may represent first-order effects, whereas differences on a hillslope and differences within a micro-drainages may represent second-order effects on T_r. This is partially supported by the similarity of the two values of θ_i at the start of rain on hillslope facets (Table II) for which the average difference is only 0·046 cm^3 cm^{-3}. For $t_t > 0$ (27%), the travel time correlated ($R^2 = 0{\cdot}39$) inversely with *a* suggesting that the travel time component of T_r may be more important for storms having high rainfall acceleration.

Soil–saturation deficit relation

The soil–saturation deficit relation explained 80% of the variance in the observed values of T_r when travel times are included (Equation (5)). If only data for $t_t = 0$ is considered, then the corresponding predictive relation for T_r could be used, with appropriate values of θ_i and θ_s, to determine the initial abstraction from a hyetograph as an alternative to deploying OFDs. This relation is similar to Equation (5), under predicts for $T_r >$ ~5 minutes, and over predicts for $T_r <$ ~5 minutes:

$$\text{Observed } T_r = 2{\cdot}03 \text{ Predicted } T_r - 5{\cdot}47,\ R^2 = 0{\cdot}79,\ \text{for } t_t = 0 \quad (6)$$

where the 95% confidence limits for the slope and intercept are ± 0.28 and ± 3.30 minutes, respectively. Saturated θ_s was assumed to be 0.49 cm^3 cm^{-3}, but varying θ_s by ± 0·05 cm^3 cm^{-3} only changed the slope in Equation (6) by about ± 6%.

Over prediction is reflected by the non-zero intercept, and there are several possible explanations. First, Equations (3a) and (3b) relating R_p to $\theta_s - \theta_i$ were developed from data collected at the two difference infiltrometer sites and not at each of the six OFD sites. Not surprisingly, these equations predict R_p at the difference infiltrometer sites (669824 and 10236) better ($R^2 = 0{\cdot}61$ and 0·26, respectively) in 2012 than they predict R_p at the OFD sites ($R^2 < 0.01$). Additionally, Equation (3a) always predicts the same value of R_p (i.e. the value associated with the single $\theta_s - \theta_i$ value at the difference infiltrometer site) for each of the three upper OFD sites, whereas given the spatial variability of soil properties, the values probably differ. Same is true for Equation (3b) and the three lower OFD sites.

Two unusual conditions may also explain why the soil–water deficit equation (Equations (5) and (6)) over predicts T_r. One was the unusually dry soil conditions (0·015–0·018 cm^3 cm^{-3}) on 5A July 2012 (Figure 6) that may have caused the reappearance of water repellency (Doerr and Thomas, 2000; Huffman *et al*., 2001). This would reduce infiltration and explain the reduction in I_a from the predicted value of 3·7 mm to the observed values of 0·41, 0·28 and 0·74 mm (Table III). The other condition was the extreme values of rainfall acceleration (1680 and 1970 mm h^{-2}) on 30A July 2012 (Figure 6). The soil-deficit equations were developed for rainfall–runoff conditions for which 90% of the rainfall accelerations were less than 1000 mm h^{-2} and thus may not be applicable for these extreme rainfall conditions.

Depression storage

Initial abstraction must satisfy the initial infiltration until ponding and the depression storage. A subset of the OFD

measurements, used to determine Equation (4), can be used to determine another empirical relation to predict $T_r^{'}$ when $t_t = 0$, and thus, determine the value of R_p that equals I_a. The relation is nearly the same as Equation (4):

$$\text{Observed } T_r^{'} = 1{\cdot}46 \text{ Predicted } T_r^{'} - 0{\cdot}38,\ R^2 = 0{\cdot}98 \text{ for } t_t = 0 \quad (7)$$

with 95% confidence limits for the slope and intercept of ± 0·05 and ± 0·75 minutes. This relation also, on average, under predicts the observed values of $T_r^{'}$, but still over predicts values for $T_r^{'} < 2$ minutes. However, time to fill depression storage, t_s, was assumed to be zero in determining Equation (7), but it may account for some of the time difference between observed and predicted values. While we did not measure t_s directly, an order of magnitude estimate can be made to assess whether it is potentially a significant process in determining $T_r^{'}$ and thus I_a. To do this, high-resolution longitudinal profiles of the micro-drainages were extracted from a data set collected using a tripod laser scanning system (Rengers *et al.*, 2012). These profiles showed that about 10% of the micro-drainages consisted of depressions with typical depths, d (in centimeters), on the order of 5 cm, lengths ranging from 15 to 45 cm, and local bed slopes that were either flat or negative. Estimates of the time ($t_s^{'} = \sqrt{(2d/a)}$) for rainfall to fill these depressions were on the order of 10 to 200 minutes, and much longer than the time difference. Whereas, estimates of the time, $t_s^{''}$, for flow in the micro-drainages (~0·5 cm deep) to fill these depressions gave 0·4 to 1·1 minutes assuming a velocity of ~6·9 cm s^{-1}. Thus, filling surface depressions appears to account for most of the time difference between observed and predicted values, but in general, it is an order of magnitude less than the ponding times, t_p (Table II). A more rigorous investigation would require high-resolution digital elevation models of hillslopes and micro-drainages to determine the spatial distribution and volumes of surface depressions.

Flow velocities

OFD measurements of unsteady flow velocities during rainstorms are all within the range of steady flow velocities published in the literature for burned or bare soils (Table III). A few maximum velocities of the leading edge of the flow (93 and 50 cm s^{-1}, upper group, 12A July 2012; and 73 cm s^{-1}, lower group, 8A July 2012, Table III) appear to be outliers. They may represent the situation when ponding at the upstream detector occurred just before ponding at the downstream detector rather than representing flow in the micro-drainage between detectors.

The maximum velocity of the hydrographic peak was 52 cm s^{-1} (upper group) and the relatively high peak velocities of 24 and 34 cm s^{-1} (lower group) were all associated with one of the most intense storm cells (5A July storm cell, maximum one-minute intensity of 101 to 104 mm h^{-1}, Table III) during the entire summer. These velocities are comparable with those reported by Nyman *et al.* (2013) and Robichaud *et al.* (2010) for burned soils. Thus, these OFD measurements of unsteady flow velocities during convective rain storms are physically realistic. Moreover, these and future OFD travel time measurements can be used with confidence to verify hydrologic models of unsteady runoff, and thus improve predictions of post-wildfire runoff.

Applications

Uncertainty exists in selecting values of model parameters to account for the effects of wildfire. OFD measurements made in burned areas can provide estimates of critical input parameters for hydrologic models and can be used to verify these models. In addition to the measurements of initial abstraction and travel times, OFDs measurements can be used to determine the critical rainfall intensity, i_r (in mm h^{-1}), at the start of runoff (Table II, column 6). This intensity can be used to estimate critical soil variables for infiltration models such as K_s (given the wetting-front suction, S_f) or S_f (given K_s). The value of S_f is probably the more important variable because it is more difficult to measure than K_s, which has been reported for fire-affected soils in the literature (Robichaud, 2000; Kinner and Moody, 2010; Nyman *et al.*, 2010; Beatty and Smith, 2013; Moody and Ebel, 2013). Normally, infiltration models must solve for time of ponding or runoff, but OFDs record this critical time. Thus, assuming that momentarily just after the start of runoff the infiltrability, f_c, (in mm h^{-1}), will equal i_r, then the Green–Ampt equation (HEC-HMS, 2000) can be written as:

$$f_c = i_r = K_s\left[1 + \frac{(\theta_s - \theta_i)S_f}{R_p}\right]. \quad (8)$$

This can be solved for the wetting-front suction, giving

$$S_f = \frac{R_p}{(\theta_s - \theta_i)}\left[\frac{i_r}{K_s} - 1\right] \quad (9)$$

To illustrate this application, we used the value of K_s (1·8 mm h^{-1}) given earlier for the upper layer of soil, and assumed that θ_i at the OFDs was equal to that at the difference infiltrometers. The computed geometric mean value of S_f was 32 mm, which is similar to that reported for sand (49·5 mm) by Rawls *et al.* (1993) and physically reasonable given the gravelly nature of the soils.

Knowledge of the excess rainfall, and hence the runoff, hinges on the accurate prediction of infiltration, which is a non-linear function of the soil–water deficit. This deficit also controls soil–water repellency. Therefore, we advocate that more *in situ* measurements of θ_i be made in burned areas, and specifically that new instrumentation be developed to measure θ_i at shallow depths (i.e. ~1–2 cm) because post-wildfire infiltration and runoff are controlled within these depths (Moody and Ebel, 2013). Soil–water deficit is a critical variable and initial values before a storm cell are needed if hydrological models are to be run in forecast mode. It is now certainly possible to telemeter these data as quasi real-time inputs to hydrologic models.

These OFD measurements coupled with θ_i measurements at shallow depths can also help to understand the redistribution of soil–water content between storm cells. Models often make crude approximation or ignore it (KINEROS2, 2014), yet one storm cell may 'prime the pump' for latter cells that may produce substantial floods even though the storm may be smaller in magnitude.

Finally, the time-to-start of runoff can be output from a hydrologic model of a burned area and compared to measurements made using OFDs. It was found in this study that time for depression storage was small relative to the time for ponding, but this might not be the case for different burned sites with different surface roughness and connectivity characteristics. These comparisons would serve as a way to verify post-wildfire hydrologic models.

Summary and Conclusions

Hydrographs of unsteady overland flow in micro-drainages on hillslopes during actual rainstorms were measured *in situ* at a sampling frequency of one second using inexpensive OFDs. These remote measurements of the time-to-start of runoff, T_r, can be telemetered and can be used to determine important quasi, real-time parameters for hydrologic models. Measurements made at multiple sites can be used to compute unsteady overland flow velocities for model verification. If T_r measurements are combined with a hyetograph, actual values of the critical runoff thresholds (initial abstraction) and critical infiltrability threshold can be determined. With additional measurements of soil–water content and saturated hydraulic conductivity, the wetting-front suction parameter can be estimated and used in the infiltration component of hydrologic models.

For the particular field site in this study, overland flow did not start simultaneously on hillslope facets and in micro-drainages as is often assumed in the development of most runoff models. Flow from upstream accounted for 27% of the initiation of runoff at OFDs. Runoff was initiated first at upstream detectors 56%, at mid-stream detectors 6%, and at downstream detectors 38% of the time. Thus, initiation of runoff exhibited a complex spatial and temporal response. It started at different times at different locations during different storm cells.

Temporally, T_r, was shown to depend on the time-to-ponding, time to fill surface depression storage, and travel time between points in the micro-drainages. At this particular field site, these times were 0·5–54, 0·4–1·1, and 0·2–14 minutes, respectively and indicate the importance of the ponding process in controlling T_r. To understand the temporal initiation of runoff from burned areas, two relations were used to model the dependence of T_r on travel time, cumulative rainfall, rainfall acceleration, and the soil–water deficit. The cumulative-rainfall relation predicted time-to-ponding, and it, combined with the travel time explained 96% of the variance in the observed values of T_r. The soil–water deficit relation explained 80% of the variance, which was probably lower than the cumulative-rainfall relation because soil–water content was only measured daily at the surface (0–1·5 cm) at two locations separated from the six OFD locations. This highlights the need to develop remote sensing instruments that are capable of measuring soil–water content at shallow depths with a time resolution compatible with that of the OFDs to improve predictions of flow initiation from burned areas.

These results describing the initiation of post-wildfire runoff are an initial attempt to understand the process during unsteady flow produced by actual rainstorms rather than simulations. They highlight the importance of the rainfall acceleration characteristic in determining the time-to-start of runoff, and the value of OFDs in determining critical threshold parameters such as initial abstraction and maximum infiltrability for hydrologic modeling. However, additional work is needed to develop instrumentation and similar relations for other sites before a more general relation can be used as a forecast tool or adopted into existing hydrologic rainfall–runoff models.

Acknowledgements—Servicing the overland flow detectors on a daily basis could not been done without the assistance of Brian Ebel, Deborah Martin, and Amanda Schmidt. Tripod-laser-scanning data was generously provided by Francis Rengers to determine topography in the micro-drainages. Reviews by Jason Kean, Kevin Schmidt, the Associated Editor, and anonymous reviewers helped immensely to clarify and to provide proper context for this scientific paper. Any use of trade, firm, or product names is for descriptive purposes only and does not imply endorsement by the US Government.

References

Abrahams AD, Li G, Krishnan C, Atkinson JF. 2001. A sediment transport equation for interrill overland flow on rough surfaces. *Earth Surface Processes and Landforms* **26**: 1443–1459. DOI. 10.1002/esp.286

Abrahams AD, Parsons AJ. 1991. Resistance to overland flow on desert pavement and its implications for sediment transport modeling. *Water Resources Research* **27**(8): 1827–1836.

Abrahams AD, Parsons AJ, Luk SH. 1986. Resistance to overland flow on desert hillslopes. *Journal of Hydrology* **88**: 343–363.

Alonistioti D, Papathanasiou C, Kasella A, Makropoulos C. 2011. Assessing the impact of forest fires on the hydrological response of urban catchments: the case of the eastern Attica region. Proceedings of the 12th International Conference of Environmental Science and Technology, Rhodes, Greece, 8–10 September 2011; A-37–A-45.

Antoine M, Javaux M, Bielders CL. 2011. Integrating subgrid connectivity properties of the micro-topography in distributed runoff models, at the interrill scale. *Journal of Hydrology* **403**: 213–223. DOI. 10.1016/j.jhydrol.2011.03.027

Assouline S, Selker JS, Parlange J-Y. 2007. A simple accurate method to predict time of ponding under variable intensity rainfall. *Water Resources Research* **43**. DOI. 10.1029/2006WR005138

Bartley R, Roth CH, Ludwig J, McJannet D, Liedloff A, Corfield J, Hawdon A, Abbott B. 2006. Runof and erosion from Australia's tropical semi-arid rangelands: influence of ground cover for differing space and time scales. *Hydrological Processes* **20**: 3317–3333. DOI. 10.1002/hyp.6334

Bautista S, Mayor ÁG, Bourakhouadar J, Bellot J. 2007. Plant spatial pattern predicts hillslope runoff and erosion in semiarid Mediterranean landscape. *Ecosystems* **10**: 987–998. DOI. 10.1007/s10021-007-9074-3

Beatty SM, Smith JE. 2013. Dynamic soil water repellency and infiltration in post-wildfire soils. *Geoderma* **192**: 160–172.

Betson RP. 1964. What is watershed runoff? *Journal of Geophysical Research* **69**: 1541–1552.

Blasch KW, Ferré PA, Christensen AH, Hoffmann JP. 2002. New field method to determine streamflow timing using electrical resistance sensors. *Vadose Zone Journal* **1**: 289–299.

Bryan RB, Yair A, Hodges WK. 1978. Factors controlling the initiation of runoff and piping in Dinosaur Provincial Park badlands, Alberta, Canada. *Zeitschrift fuer Geomorphologie N.F., Suppl. Bd* **29**: 151–168.

Bunte K, Poesen J. 1994. Effects of rock fragment size and cover on overland flow hydraulics, local turbulence and sediment yield on an erodible soil surface. *Earth Surface Processes and Landforms* **19**: 115–135.

Carey SK, DeBeer CM. 2008. Rainfall–runoff hydrograph characteristics in a discontinuous permafrost watershed and their relation to ground thaw. Proceedings Ninth International Conference on Permafrost; 233–238.

CASC2D. 2014. The CASC2D-SED watershed model. http://www.engr.colostate.edu/~pierre/ce_old/Projects/CASC2D-SED%20Web%20site%20082506/CASC2D-SED-Home.htm [17 November 2014].

Chu X, Mariño MA. 2005. Determination of ponding condition and infiltration into layered soils under unsteady rainfall. *Journal of Hydrology* **313**: 195–207.

Clothier B, White J. 1981. Measurement of sorptivity and soil water diffusivity in the field. *Soil Science Society of America Journal* **45**: 241–245.

Cydzik K, Hogue TS. 2009. Modeling postfire response and recovery using the Hydrologic Engineering Center Hydrologic Modeling System (HEC-HMS). *Journal of the American Water Resources Association* **45**(3): 702–714.

Darboux F, Gascuel-Odoux C, Davy P. 2002. Effects of surface water storage by soil roughness on overland-flow generation, *Earth Surface Processes and Landforms* **27**: 223–233.

Diskin MH, Nazimov N. 1996. Ponding time and infiltration capacity variation during steady rainfall. *Journal of Hydrology* **178**: 369–380.

Doerr SH, Thomas AD. 2000. The role of soil moisture in controlling water repellency: new evidence from forest soils in Portugal. *Journal of Hydrology* **231–232**: 134–147.

Douglas MW, Maddox RA, Howard K, Reyes S. 2004. The North American Monsoon. Reports to the Nation on our Changing Planet. NOAA/National Weather Service. http://www.cpc.noaa.gov/products/outreach/Report-to-the-Nation-Monsoon_aug04.pdf

Dunne T. 1978. Field studies of hillslope flow processes. In Hillslope Hydrology, Kirkby MJ (ed.). John Wiley & Sons: Chichester; 227–293.

Dunne T, Aubry BF. 1986. Evaluation of Horton's theory of sheetwash and rill erosion on the basis of field experiments. In Hillslope Processes, Abrahams AD (ed.). George Allen & Unwin; London; 31–53.

Dunne T, Dietrich WE. 1980. Experimental investigation of Horton overland flow on tropical hillslopes, 2. Hydraulic characteristics and hillslope hydrographs. *Zeitschrift fuer Geomorphologie N.F., Suppl.-Bd* **35**: 60–80.

Ebel BA, Moody JA, Martin DA. 2012. Hydrologic conditions controlling runoff generation immediately after wildfire. *Water Resources Research* **48**: W03529. DOI. 10.1029/2011WR011470

Elliott JG, Smith ME, Friedel MJ, Stevens MR, Bossong CR, Litke DW, Parker RS, Costello C, Wagner J, Char SJ, Bauer MA, Wilds SR. 2005. Analysis and Mapping of Post-fire Hydrologic Hazards for the 2002 Hayman, Coal Seam, and Missionary Ridge Wildfires, Colorado, US Geological Survey, Scientific Investigations Report 2004–5300. US Geological Survey: Reston, VA; 104 pp.

Emmett WW. 1970. The Hydraulic of Overland Flow on Hillslopes, US Geological Survey Professional Paper 662-A, US Geological Survey: Reston, VA; 68 pp.

Esteves M, Faucher X, Galle S, Vauclin M. 2000. Overland flow and infiltration modelling for small plots during unsteady rain: numerical results versus observed values. *Journal of Hydrology* **228**: 265–282.

Foltz RB, Robichaud PR, Hakjun R. 2009. A Synthesis of Post-fire Road Treatments for BAER Teams: Methods, Treatment Effectiveness and Decision Making Tools for Rehabilitation, General Technical Report RMRS-GTR-228. US Department of Agriculture, Forest Service, Rocky Mountain Research Station: Fort Collins, CO; 152 pp.

Gilley JE, Kottwitz ER, Wieman GA. 1992. Darcy–Weisbach roughness coefficients for gravel and cobble surfaces. *Journal of Irrigation and Drainage Engineering. ASCE* **118**: 104–112.

van Genuchten MT, Leij FJ, Yates SR. 1991. The RETC Code for Quantifying the Hydraulic Functions of Unsaturated Soils, EPA/600/2091/065, Robert S. Kerr Environmental Research Laboratory, Office of Research and Development, US Environmental Protection Agency: Ada, OK.

Goulsbra CS, Lindsay JB, Evans MG. 2009. A new approach to the application of electrical resistance sensors to measuring the onset of ephemeral streamflow in wetland environments. *Water Resources Research* **45**: W09501. DOI. 10.1029/2009WR007789

Green WA, Ampt GA. 1911. Studies on soil physics: 1. The flow of air and water through soils. *Journal of Agriculture Science* **4**: 1–24.

Hawkins RH, Ward TJ, Woodward E, Van Mullem JA. 2010. Continuing evolution of rainfall–runoff and the curve number precedent. Proceedings, 2nd Joint Federal Interagency Conference, Las Vegas, NV, 27 June–1 July 2010; 12 pp.

Henderson FM, Wooding RA. 1964. Overland flow and groundwater flow from a steady rainfall of finite duration. *Journal of Geophysical Research* **69**(8): 1531–1540.

Horton RE. 1939. Analysis of runoff-plot experiments with varying infiltration capacity. *Eos, Transactions American Geophysical Union* **20** (Part IV): 696–711.

Huizinga RJ. 2014. An Initial Abstraction and Constant Loss Model, and Methods for Estimating Unit Hydrographs, Peak Streamflows, and Flood Volumes for Urban Basins in Missouri. US Geological Survey, Scientific Investigation Report 2014–5193. US Geological Survey: Reston, VA; 59 pp.

Huffman EL, MacDonald LH, Stednick JD. 2001. Strength and persistence of fire-induced soil hydrophobicity under ponderosa and lodgepole pine, Colorado Front Range. *Hydrological Processes* **15**: 2877–2892. DOI. 10.1002/hyp.379

Hydrologic Engineering Center Hydrologic Modeling System (HEC-HMS). 2000. Hydrologic Modeling System, HEC-HMS, Technical Reference Manual. US Army Corps of Engineers, Hydrologic Engineering Center. http://www.hec.usace.army.mil/software/hec-hms/documentation.aspx [17 November 2014].

Julien PY, Moglen GE. 1990. Similarity and length scale for spatially varied overland flow. *Water Resources Research* **26**(8): 1819–1832.

Julien PY, Saghafian B, Ogden FL. 1995. Raster-based hydrologic modeling of spatially-varied surface runoff. *Water Resources Bulletin* **21**(3): 523–536.

KINEROS2. 2014. The soil infiltration model in KINEROS2. http://www.tucson.ars.ag.gov/kineros [17 November 2014].

Kinner DA, Moody JA. 2010. Spatial variability of steady-state infiltration into a two-layer soil system on burned hillslopes. *Journal of Hydrology* **381**: 322–332. DOI. 10.1016/j.jhydrol.2009.12.004

Kirkby MJ. 2011. A personal synthesis. In Hydro-geomorphology, Erosion and Sedimentation, IAHS Publication, Benchmark Papers in Hydrology 6. IAHS Press: Wallingford; 1–36.

Kirkby M, Callan J, Weyman D, Wood J. 1976. Measurement and Modelling of Dynamic Contributing Areas in Very Small Catchments, Working Paper No. 167. School of Geography, University of Leeds: Leeds; 39 pp.

Kumke T, Mullins CE. 1997. Field measurement of time to ponding. *Soil Use and Management* **13**: 24–28.

Liu H, Lei TW, Zhao J, Yuan CP, Fan YT, Qu LQ. 2011. Effects of rainfall intensity and antecedent soil water content on soil infiltrability under rainfall conditions using the run off-on-out method. *Journal of Hydrology* **396**: 24–32. DOI. 10.1016/j.jhydrol.2010.10.028

Mein RG, Larson CL. 1973. Modeling infiltration during a steady rain. *Water Resources Research* **9**(2): 384–394.

Mitsudera M, Kamata Y, Nakane K. 1984. Effect of fire on water and major nutrient budgets in forest ecosystems, III. Rainfall interception by forest canopy. *Japanese Journal of Ecology* **34**: 15–25.

Moody JA, Ebel BA. 2012a. Hyper-dry conditions provide new insights into the cause of extreme floods after wildfire. *Catena* **93**: 58–63. DOI. 10.1016/j.catena.2012.01.006

Moody JA, Ebel BA. 2012b. Difference infiltrometer: a method to measure temporally variable infiltration rates during rainstorms. *Hydrological Processes* **26**: 3312–3318. DOI. 10.1002/hyp.9424

Moody JA, Ebel BA. 2013. Infiltration and runoff generation processes in fire-affected soils. *Hydrological Processes* **28**: 3432–3453. DOI. 10.1002/hyp.9857

Moody JA, Martin DA. 2009. Forest fire effects on geomorphic processes. In Fire Effects on Soils and Restoration Strategies, Cerdà A, Robichaud PR (eds). Science Publishers: Enfield, NH; 41–79.

Moreland DC, Moreland RE. 1975. Soil Survey of Boulder County Area, Colorado. US Department of Agriculture, Natural Resources Conservation Service: Washington, DC; 91 pp.

Natural Resources Conservation Service (NRCS). 2004. Estimation of Direct Runoff from Storm Rainfall, National Engineering Manual, Chapter 10, 210-VI-NEH. USDA Natural Resources Conservation Service. http://www.nrcs.usda.gov/wps/portal/nrcs/detailfull/national/water/?cid=stelprdb1043063 [17 November 2014].

Natural Resources Conservation Service (NRCS). 2010. Time of Concentration, National Engineering Manual, Chapter 15, 210-VI-NEH. USDA Natural Resources Conservation Service. http://www.nrcs.usda.gov/wps/portal/nrcs/detailfull/national/water/?cid=stelprdb1043063 [17 November 2014].

Nyman P, Sheridan GJ, Lane PNJ. 2010. Synergistic effects of water repellency and macropore flow on the hydraulic conductivity of a burned forest soil, southeast Australia. *Hydrological Processes* **24**: 2871–2887.

Nyman P, Sheridan GJ, Moody JA, Smith HG, Noske PJ, Land PNJ. 2013. Sediment availability on burned hillslopes. *Journal of Geophysical Research, Earth Surface* **118**: 1–17. DOI. 10.1002/jgrf.20152

Orchard CM, Lorentz SA, Jewitt GPW, Chaplot VAM. 2013. Spatial and temporal variations of overland flow during rainfall events and in relation to catchment conditions. *Hydrological Processes* **27**: 2325–2338. DOI. 10.1002/hyp.9217

Parlange JY, Smith RE. 1976. Ponding time for variable rainfall rates. *Canadian Journal of Soil Science* **56**: 121–123.

Parlange JY, Lisle I, Braddock RD, Smith RE. 1982. The three-parameter infiltration equation. *Soil Science* **133**(6): 337–341.

Parsons AJ, Wainwright J, Abrahams AD. 1996. Runoff and erosion on semi-arid hillslopes. In Advances in Hillslope Processes, *Volume* **2**, Anderson MG, Brooks SM (eds). John Wiley & Sons: Chichester; chapter 48, 1061–1078.

Pepin N. 2000. Twentieth-century change in the climate record for the Front Range, Colorado, U.S.A. *Arctic, Antarctic, and Alpine Research* **32**(2): 135–146.

Phillips JD. 1992. Deterministic chaos in surface runoff. In Overland Flow, Hydraulic and Erosion Mechanics, Parsons AJ, Abrahams AD (eds). Chapman & Hall: New York; chapter 8, 177–197.

Ponce VM, Shetty AV. 1995. A conceptual model of catchment water balance: 1. Formulation and calibration. *Journal of Hydrology* **173**: 27–40.

Rawls WJ. Ahuja LR, Brakensiek DL, Shirmohammadi A. 1993. Infiltration and soil water movement. In Handbook of Hydrology, Maidment DR (ed.), McGraw-Hill: San Francisco, CA; chapter 5, 5-1–5-51.

Rauws G 1988. Laboratory experiments on resistance to overland flow due to composite roughness. *Journal of Hydrology* **103**: 37–52.

Rengers F, Tucker G, Moody JA. 2012. Quantifying Post-Wildfire Erosion Patterns Using Terrestrial LiDAR. Poster. American Geophysical Union: San Francisco, CA; December 5, 2012.

Robichaud PR. 2000. Fire effects on infiltration rates after prescribed fire in Northern Rocky Mountain forests, USA. *Journal of Hydrology* **231–232**: 220–229.

Robichaud PR, Wagenbrenner JW, Brown RE. 2010. Rill erosion in natural and disturbed forests: 1. Measurements. *Water Resources Research* **46**: W10506. DOI. 10.1029/2009WR008314

Schmidt KM, Hanshaw MN, Howle JF, Kean JW, Staley DM, Stock JD, Bawdeng W. 2011. Hydrologic conditions and terrestrial laser scanning of post-fire debris flows in the San Gabriel, Mountains, Ca, U. S.A. *Italian Journal of Engineering Geology and Environment, Proceedings of 5th International Conference on Debris-Flow Hazards 'Mitigation, Mechanics, Prediction and Assessment'* 583–593. DOI. 10.4408/IJEGE.2011-03.B-064

Sen S, Srivastava P, Dane JH, Yoo KH, Shaw JN. 2010. Spatial-temporal variability and hydrologic connectivity of runoff generation areas in a North Alabama pasture—implications for phosphorus transport. *Hydrological Processes* **24**: 342–356. DOI: 10.1002/hyp.7502

Sheridan GJ, Land PNJ, Noske PJ. 2007. Quantification of hillslope runoff and erosion processes before and after wildfire in a wet *Eucalyptus* forest. *Journal of Hydrology* **343**: 12–28. DOI. 10.1016/j.jhydrol.2007.06.005

Šimùnek J, Šejna M, Saito H, Sakai M, van Genuchten MT. 2008. The HYDRUS-1D Software Package for Simulating the Movement of Water, Heat, and Multiple Solutes in Variably Saturated Media, Version 4.08, HYDRUS Software Series 3. Department of Environmental Sciences, University of California Riverside: Riverside, CA; 330.

Smith RE. 2002. Infiltration Theory for Hydrologic Applications, Water Resources Monograph 15. American Geophysical Union: Washington, DC; 212 pp.

Smith RE, Goodrich DC. 2005. Rainfall excess overland flow. In Encyclopedia of Hydrological Sciences, Anderson MG (ed.). John Wiley & Sons: Chichester; chapter 111, 1707–1718.

Springer EP, Hawkins RH. 2005. Curve Number and Peak Flow Responses Following the Cerro Grande Fire on a Small Watershed, Los Alamos National Laboratory, LA-UR-05-0552. Los Alamos National Laboratory: Los Alamos, NM; 12 pp.

Srinivasan MS, Gburek WJ, Hamlett JM. 2002. Dynamics of stormflow generation – a hillslope-scale field study in east-central Pennsylvania, USA. *Hydrological Processes* **16**: 649–665. DOI. 10.1002/hyp.311

Stone JJ, Lane LJ, Shirley ED, Hernandez M. 1995. Hillslope Surface Hydrology. USDA–Water Erosion Prediction Project. US Department of Agriculture: Fort Collins, CO; chapter 4, 4-1–4-20. http://www.ars.usda.gov/Research/docs.htm?docid=18073 [17 November 2014].

Topp GC, Ferré PA. 2002. Methods for measurement of soil water content: thermogravimetric using convective oven-drying. In Methods of Soil Analysis. Part 4 Physical Methods, Soil Science Society of America Book Series: 5, Dane JH, Topp GC (eds). Soil Science Society of America: Madison, WI; 422–424.

US Department of Agriculture (USDA). 2010. Soil Survey Staff. US Department of Agriculture, Natural Resource Conservation Service: Washington, DC. http://websoilsurvey.nrcs.usda.gov/

Water Erosion Prediction Project (WEPP). 2014. USDA-Water Erosion Prediction Project. US Department of Agriculture. http://www.ars.usda.gov/Research/docs.htm?docid=18073 [17 November 2014].

Woodward DE, Hawkins RH, Jiang R. Hjelmfelt AT jr, Van Mullen JA, Quan QD. 2003. Runoff curve number method: examination of the initial abstraction ratio. Proceedings of the World Water and Environmental Resources Congress 2003 and Related Symposia, Bizier P, DeBarry PA (eds). Environmental and Water Resources Institute, ASCE, 23–26 June 2003, Philadelphia, PA.

Woolhiser DA. 1975. Simulation of unsteady overland flow. In Unsteady Flow in Open Channels, Mahmood K, Yevjevich VM (eds). Water Resources Publications: Fort Collins, CO; 485–508.

Woolhiser DA, Smith RE, Giraldez J-V. 1996. Effects of spatial variability of saturated hydraulic conductivity on Hortonian overland flow. *Water Resources Research* **32**(3): 671–678.

WRF-Hydro. 2014. The WRF-Hydro Model Technical Description and User's Guide, version 1.0, NCAR Technical Document. Gochis DJ, Yu W, Yates DN (eds). National Center for Atmospheric Research: Boulder, CO; 120 pp. http://www.ral.ucar.edu/projects/wrf_hydro/ [16 November 2014].

Xue J, Gavin K. 2008. Effect of rainfall intensity on infiltration into partly saturated slopes. *Geotechnical and Geological Engineering* **26**: 199–209.

Yair A, Sharon D, Lavee H. 1980. Trends in runoff and erosion processes over an arid limestone hillside, northern Negev, Israel. *Hydrological Sciences* **25**: 243–255.

Yuan Y, Nie W, McCutcheon SC, Taguas EV. 2014. Initial abstraction and curve numbers for semiarid watersheds in Southeastern Arizona. *Hydrological Processes* **28**(3): 774–783. DOI. 10.1002/hyp.9592

Zimmermann B, Zimmermann A, Turner BL, Francke T, Elsenbeer H. 2014. Connectivity of overland flow by drainage network expansion in a rain forest catchment. *Water Resources Research* **50**(2): 1457–1473. DOI. 10.1002/2012WR012660

